Proc. Natl. Acad. Sci. USA
Vol. 93, pp. 734–738, January 1996
Immunology

Crystallographic analysis of endogenous peptides associated with HLA-DR1 suggests a common, polyproline II-like conformation for bound peptides

(immunology/major histocompatibility complex/peptide binding)

THEODORE S. JARDETZKY*†, JERRY H. BROWN*‡§, JOAN C. GORGA¶, LAWRENCE J. STERN*‡‖, ROBERT G. URBAN*, JACK L. STROMINGER*, AND DON C. WILEY*,‡,**

*Department of Molecular and Cellular Biology and ‡Howard Hughes Medical Institute, Harvard University, 7 Divinity Avenue, Cambridge, MA 02138; §Rosenstiel Research Center, Brandeis University, 415 South Street, Waltham, MA 02254; ¶Department of Pediatrics, Children's Hospital of Pittsburgh, 6130 Rangos Research Building, 3705 Fifth Avenue, Pittsburgh, PA 15213; ‖Department of Chemistry, Massachusetts Institute of Technology, Cambridge, MA 02139; and †Department of Biochemistry, Molecular Biology and Cell Biology, Northwestern University, Evanston, IL 60208

Contributed by Don C. Wiley, September 15, 1995

ABSTRACT **The structure of the human major histocompatibility complex (MHC) class II molecule HLA-DR1 derived from the human lymphoblastoid cell line LG-2 has been determined in a complex with the *Staphylococcus aureus* enterotoxin B superantigen. The HLA-DR1 molecule contains a mixture of endogenous peptides derived from cellular or serum proteins bound in the antigen-binding site, which copurify with the class II molecule. Continuous electron density for 13 amino acid residues is observed in the MHC peptide-binding site, suggesting that this is the core length of peptide that forms common interactions with the MHC molecule. Electron density is also observed for side chains of the endogenous peptides. The electron density corresponding to peptide side chains that interact with the DR1-binding site is more clearly defined than the electron density that extends out of the binding site. The regions of the endogenous peptides that interact with DR1 are therefore either more restricted in conformation or sequence than the peptide side chains or amino acids that project out of the peptide-binding site. The hydrogen-bond interactions and conformation of a peptide model built into the electron density are similar to other HLA-DR–peptide structures. The bound peptides assume a regular conformation that is similar to a polyproline type II helix. The side-chain pockets and conserved asparagine residues of the DR1 molecule are well-positioned to interact with peptides in the polyproline type II conformation and may restrict the range of acceptable peptide conformations.**

Major histocompatibility complex (MHC) class II molecules present peptide antigens to T cells in the generation of an immune response (1). Antigenic peptides are derived from exogenous proteins, which are processed into peptide fragments by antigen-presenting cells. MHC class II molecules also bind self-peptides derived from cellularly produced proteins. Self-peptides isolated from purified class II molecules, including HLA-DR1 (2, 3), vary in length from ≈13 to 25 amino acids. This length variability contrasts with the shorter peptides found associated with MHC class I molecules, which are generally 9–11 amino acids long (4–6). For MHC class I molecules the N and C termini of peptides are typically bound in pockets at each end of the peptide-binding site (7–9), whereas for the MHC class II molecules, HLA-DR1 and HLA-DR3, peptides are free to extend out both ends of the binding site. Instead of the network of hydrogen bonds found between the MHC class I molecule and the peptide N and C termini, class II has evolved an alternative hydrogen-bonding interaction along the length of the peptide main chain (10, 11), allowing the termini to extend out of the binding site. This hydrogen-bonding scheme provides interactions with main-chain atoms, which are present in all peptides, and is likely important for the tight binding of peptides of variable sequence (12).

Analysis of the electron density corresponding to the mixture of self-peptides bound to MHC class I molecules has provided insights into general aspects of the MHC class I–peptide interaction. In the case of HLA-B27 (8, 9, 13), this provided the first interpretation of the MHC–peptide interactions, whereas for HLA-Aw68 (14), the absence of electron density for the central peptide residues indicated significant conformational heterogeneity, subsequently observed in five different HLA-A2–single peptide structures (9). The electron density corresponding to a mixture of self-peptides bound to HLA-DR1 isolated from the LG-2 B-lymphoblastoid cell line has improved during refinement of the HLA-DR1–*Staphylococcus aureus* enterotoxin B (SEB) complex. The electron density is continuous and interpretable throughout the peptide-binding site for 13 amino acid residues. Side-chain density is observed for most of the amino acid positions corresponding to residues pointing into pockets of the HLA-DR1 molecule. Three peptide amino acid positions that point out of the peptide-binding site show more complex density, suggesting a mixture of possible amino acid side chains and conformations. After the 13th residue, the electron density bifurcates, suggesting that longer peptides become disordered as they exit the peptide-binding site. The clarity of the peptide main-chain and side-chain density suggests a core binding length of 13 amino acids for peptides that bind to HLA-DR1. The peptide conformation, which has ϕ and ψ angles close to those of a polyproline type II (ppII) helix, is similar to that observed in the crystal structure of an influenza hemagglutinin peptide bound to the HLA-DR1 molecule (11) and the invariant-chain class II-associated Ii peptides (CLIP) peptide complex with HLA-DR3 (15). Six of the potential hydrogen bonds to the peptide main chain involve conserved asparagine residues of the MHC molecule. These conserved asparagines form 9- and 11-membered rings, bidentate hydrogen bonds that in combination with MHC pockets may serve to restrict the possible peptide main-chain conformations. The conserved MHC asparagine residues are poised to interact with the helical repeat of the ppII peptide conformation, placing a common conformational constraint on a repeating tripeptide unit, in which the central amino acid always points out of the peptide-binding

The publication costs of this article were defrayed in part by page charge payment. This article must therefore be hereby marked "*advertisement*" in accordance with 18 U.S.C. §1734 solely to indicate this fact.

Abbreviations: MHC, major histocompatibility complex; SEB, *Staphylococcus aureus* enterotoxin B superantigen; ppII, polyproline type II; HA, hemagglutinin; CLIP, class II-associated Ii peptides.

**To whom reprint requests should be addressed.

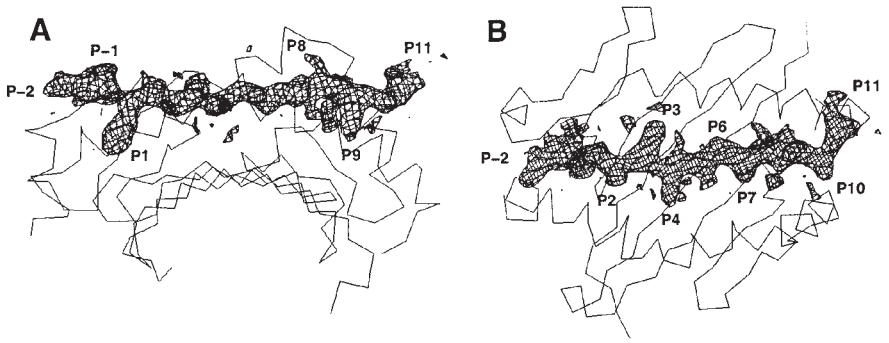

FIG. 1. Electron density observed for self-peptides bound to HLA-DR1. (*A*) Side. (*B*) Top A $2|F_0-F_c|\phi_{ave}$ electron-density map calculated after 10 cycles of noncrystallographic symmetry averaging and solvent flattening, starting with model phases before any peptide atoms were built. Density is presented within a cover radius from modeled peptide atoms. Some HLA-DR1 side-chain density is also evident for residues forming H bonds to peptide atoms in peptide residues P4, P5, and P8.

site. These observations indicate that the variability in the conformation of peptides bound to HLA-DR molecules is more restricted than that observed for the MHC class I molecule HLA-A2 (9) and the ppII conformation may be a general feature of peptides bound to MHC class II molecules.††

MATERIALS AND METHODS

The structure determination of the DR1–SEB complex has been described (16). Crystals were harvested in well buffer (16) containing an additional 2% PEG 4000. Before flash cooling for data collection (to −165°C), crystals were soaked in harvest buffer with glycerol, in 2% steps (1 hr each), to a final concentration of 10% (vol/vol) glycerol. Synchrotron data from the crystal form that diffracts to the highest resolution ($P2_12_12_1$, Form I in ref. 16) were collected to 2.7 Å resolution (R_{merge} = 5.7%) (16).

The HLA-DR1 structure was determined by averaging three crystal forms (10). A polyalanine model for the SEB portion of the complex was built at 4.3-Å resolution, after 4-fold, noncrystallographic symmetry averaging between two different DR1–SEB space groups (16). This model provided phases for 3.5-Å omit maps of the SEB structure using the high-resolution synchrotron data, and the model was improved by cycles of building, XPLOR refinement (17), and extension to 2.7-Å resolution. XPLOR cycles typically included positional refinement with harmonic constraints placed on Cα positions, followed by unconstrained positional refinement. Progress was monitored by the free *R* factor (17), using 10% of the reflections removed before any refinement. During initial stages an overall temperature factor was used for all atoms of the structure. Eventually, any unconstrained positional refinement led to increases in the R_{free}, although the crystallographic *R* factor continued to decrease. Refinement of restrained individual temperature factors at this stage showed large differences in the mean temperature factors for the DR1 and SEB regions of the model, indicating a global difference reflecting the disorder of SEB in the crystal lattice. However, individual temperature factors were not used in subsequent refinement at this stage. To verify that the SEB molecule was built correctly three tests were undertaken. (*i*) A series of simulated annealing SEB omit maps were generated from the DR1–SEB structure, and the resulting maps were inspected. (*ii*) An independently refined model of the DR1–hemagglutinin (HA) peptide complex (11) was used to calculate starting phases for iterative 2-fold non-crystallographic-symmetry averaged maps. The refined DR1–HA model provided better starting phases than the experimental phases and had no prior bias for the SEB model. (*iii*) Two independently refined models of the DR1 molecule and the SEC3 (18) molecule were used in a full molecular replacement search with the program AMORe (19) and to generate a series of SEB omit maps. These three tests all verified both the placement of the SEB molecule in the crystal and the relative disorder of SEB compared to DR1. Subsequently, at the start of a refinement cycle after manual rebuilding, 12 ≈90-amino acid domains of the structure were given grouped temperature factors to account for the relative disorder in different regions of the complex. Initially one overall temperature factor was assigned per domain and then later shifted to two temperature factors (one main chain, one side chain). This shift allowed further positional refinement at early stages, as observed by decreases in R_{free}. Eventually, significant reduction in the R_{free} could only be obtained by cycles of positional refinement, during which harmonic constraints were placed on the Cα positions of poorly determined DR1 loops and SEB. This result is consistent with these regions of the model being less constrained by the diffraction data and therefore subject to overfitting. Individual restrained *B*-factor refinement was done at the end of a cycle of XPLOR refinement.

The current model has a crystallographic *R* factor of 25.7% and a free *R* factor of 32.7%, with good geometry and does not include any water molecules (16). The electron-density maps shown are calculated with $2|F_o-F_c|\phi_{ave}$ coefficients before building peptide into the MHC-binding-site density. Subsequently, a 13-amino acid polyalanine model for the peptide was included in the refinement of the DR1–SEB model, lowering the R_{free}. The average temperature factor for the main-chain atoms of the first 11 peptide residues is 36 Å^2 (comparable to the DR1 molecule).

RESULTS AND DISCUSSION

Peptide Electron Density. Fig. 1 shows the endogenous peptide electron density observed in the HLA-DR1 peptide-binding site. The peptide electron density shown has no model bias and is readily interpretable for a segment of 13 amino acids extending out both ends of the DR1 peptide-binding site (10). Additional density at the C terminus of the peptide (to the right in Figs. 1 and 2) is observed at lower contour levels, consistent with the observation that longer endogenous peptides are found bound to DR1 (3).

Electron density for side chains is evident for most peptide amino acids (Fig. 1 *A* and *B*). The large side-chain electron density near the peptide N terminus is labeled P1 and corresponds to the anchoring tyrosine in the DR1–HA structure (11). Positions labeled P1–P4, P7, and P9 in Fig. 1 have

††The atomic coordinates and structure factors have been deposited in the Protein Data Bank, Chemistry Department, Brookhaven National Laboratory, Upton, NY 11973 (ENTRY ISEB).

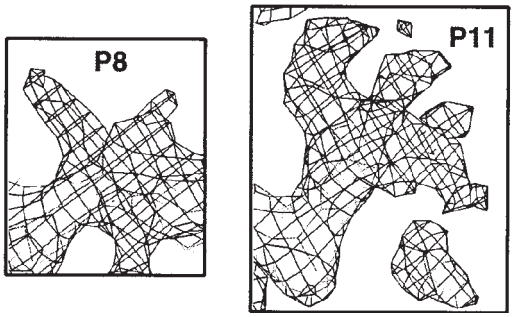

FIG. 2. Electron density observed at peptide positions P8 and P11. Position P8 points out of the peptide-binding site and shows density consistent with a mixture of side-chain residues or rotamer conformations. The C-terminal region corresponds to P11. The bifurcated density suggests that peptides longer than 13 amino acids are not restrained by the peptide-binding site and may assume different or multiple conformations.

extensions of density that are monomorphic and interpretable as side chains. Positions P-2, P5, P6, and P10 show little or no side-chain density (Fig. 1 *A* and *B*), which could be due to either the predominance of small amino acids at these positions or heterogeneity in sequence or conformation at these sites. Finally, positions P-1, P8, and the C terminus (P11) have very complex density (Figs. 1 and 2). For P-1 and P8, this could be due to a mixture of different side chains from different peptides or the structural heterogeneity of different side-chain rotamers. For the C terminus of the peptide, the complexity of the density is consistent with longer peptides being able to extend out of the binding site in different directions.

Primary amino acid preferences at four peptide positions have been identified by M13 phage-display selection and sequence analysis of peptides that bind HLA-DR1 (20–22). These peptide residues correspond to positions P1, P4, P6, and P9 of the endogenous peptide electron density shown in Fig. 1. Each position has side-chain electron density that can accommodate the amino acids in the HLA-DR1 peptide-binding motifs. Position P1, which is the most important HLA-DR1 anchor residue, is preferentially tyrosine or phenylalanine (21, 23) and has large aromatic side-chain density (Fig. 1). Position P4 has smaller side-chain electron density than P1, which is more consistent with methionine or leucine (Fig. 1). Position P6 has minimal side-chain density, in keeping with a preference for alanine, serine, or glycine. Finally, position P9, where leucine, methionine, or alanine is preferred, has electron density that can accommodate a leucine residue. The association of peptide residues P1, P4, P6, and P9 with pockets of the DR1 molecule was similarly observed in the DR1–HA peptide structure (11). The observed electron density is not easily assigned to one of the predominant peptides found bound to HLA-DR1 (3). We have therefore built a model peptide containing a minimal HLA-DR1 peptide-binding motif (NH_2-AAYAAMAAAALAA-COOH) into the endogenous peptide electron density. Other side chains from the endogenous peptide density are of similar high quality (e.g., P2 and P3 in Fig. 1). The quality of the electron density may result from the conformational superposition of similar peptides. As binding of SEB and crystallization may select for a subset of endogenous peptides, further interpretation of the side-chain density would require sequencing of the peptides incorporated into the crystals.

Peptide Conformation and Interactions. Fig. 3 emphasizes the ppII-like conformation of the peptide in the DR1 binding site. The left-handed helical twist is shown by connecting the positions of the C-β atoms of each amino acid in the modeled peptide. The ppII conformation is most evident in residues P1–P11, where three C-β atoms (P2, P5, P8) point out of the binding site. The black C-β atoms in Fig. 3 correspond to motif

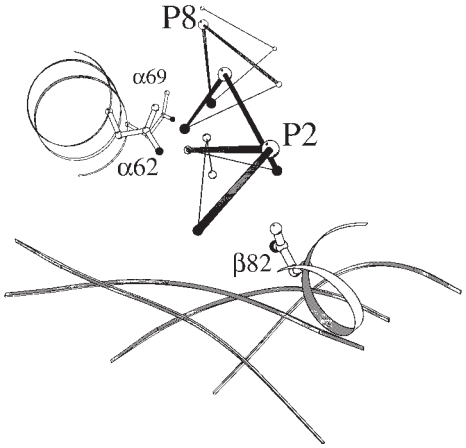

FIG. 3. Peptide main-chain conformation and DR1 asparagine residues. C-β atoms of the peptide are drawn and connected by solid rods or lines, generating a representation of the ppII peptide conformation similar to that in ref. 24. C-β atoms of P2, P5, and P8 are grey and point out of the peptide-binding site. The adjacent peptide bonds of P2, P5, and P8 (dark rods) interact with asparagine residues (α62, α69, and β82) of the DR1 molecule. The C-β atoms of P1, P4, P6, and P9 (black) correspond to the amino acids that form the major DR1 peptide-binding motif. Fig. 3 was generated with the program MOLSCRIPT (25).

positions that point into DR1 pockets (P1, P4, P6, and P9). Peptide residues at positions P3 and P7 also interact with HLA-DR1 pockets, which in some peptides could provide additional binding energy. The observed ϕ and ψ angles that correspond to this peptide conformation are relatively restricted and regular. The mean peptide ϕ and ψ angles are near $-80°$ and 130°, respectively, which are similar to the values observed for ppII helices (26) (Fig. 4). Corresponding average values for a ppII helix are indicated to the left of the graph by arrows.

Fourteen potential hydrogen bonds are observed in the complex with endogenous peptides (Fig. 5). Of these, six are bidentate hydrogen bonds involving DR1 asparagines (α62, α69, and β82), which form 9- (β82) and 11-membered (α62, α69) ring structures between the peptide main-chain atoms and the DR1 amide side-chain atoms. Similar hydrogen bond interactions are observed in other protein structures (27). The mean and SD of the ϕ/ψ angles observed for residues whose main-chain atoms form hydrogen bonds to amide side chains were calculated, using the data from refined protein structures found in table 4 of Le Questel *et al.* (27). The mean angles calculated from 32 examples from proteins in the Protein Data Bank for both the 9- and 11-membered ring motifs are similar, with overall averages of $\langle\phi\rangle = -93° \pm 25°$ and $\langle\psi\rangle = 134° \pm 15°$. Both hydrogen-bonding ring structures involve adjacent peptide bonds and therefore the same ϕ/ψ angles of the central amino acid of a tripeptide segment. The averages and SDs are plotted as boxes in Fig. 4, which emphasizes the overlap between the Protein Data Bank bidentate-hydrogen bond ϕ/ψ angles and the DR1-bound peptide ϕ/ψ angles. These ϕ/ψ angles can be compared to the average ϕ/ψ angles for those residues involved in β-sheet interactions in other regions of the DR1 molecule itself, which are $\langle\phi\rangle = -122 \pm 23°$ and $\langle\psi\rangle = 135 \pm 14°$. Therefore, the formation of the bidentate hydrogen bonds between asparagines α62, α69, and β82 and the peptide main chain may confer a preference of the MHC binding site for extended peptide conformations that are similar to the ppII conformation.

Figs. 3 and 5 also show the distribution of asparagine hydrogen bonds to the peptide within the DR1 peptide-binding site. In Fig. 5, the amide bonds of the peptide are represented as solid planes. Each of the three DR1 asparagines interacts

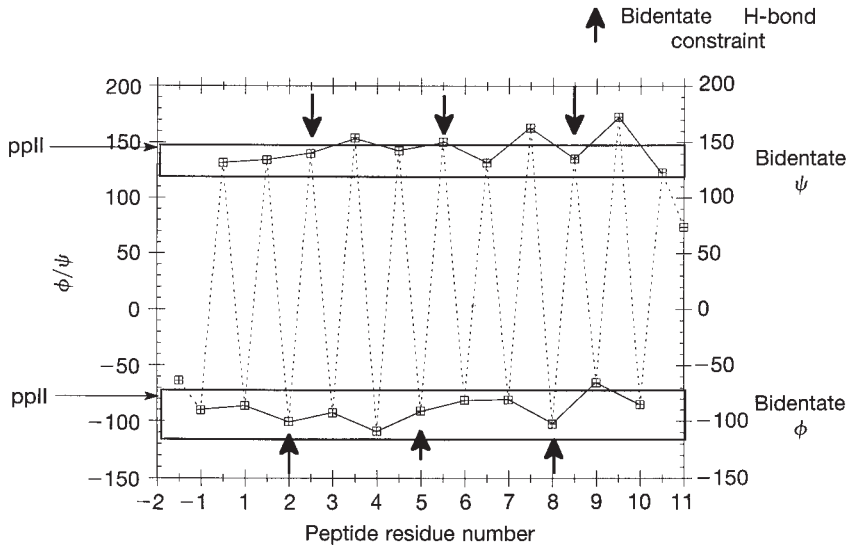

FIG. 4. Plot of the ϕ/ψ angle of the model peptide as a function of peptide residue number. Also shown are the range of the SDs about the mean of the ϕ/ψ angles observed for residues involved in amide side-chain to main-chain interactions (boxed) in the Protein Data Bank (27) and the mean ϕ/ψ values for ppII helices [ppII arrows to the left (26)]. The heavy arrows mark peptide-bond interactions with conserved asparagine residues.

with a subset of three residues of the bound peptide, by forming hydrogen bonds to the planar peptide bonds around a central amino acid. Asn-β82 interacts with the peptide bonds between P1 and P3, Asn-α62 interacts with the peptide bonds between P4 and P6, and Asn-α69 interacts with the peptide bonds between P7 and P9. In each tripeptide, the central residue (P2, P5, and P8; Fig. 3) points out of the peptide-binding site. One amide plane without hydrogen bond interactions lies between each pair of the bidentate interactions (residues P3–P4 and P6–P7), which leaves only two of the eight central amide planes of the peptide-binding site without a direct interaction with one of the asparagine residues.

As seen in Fig. 5, the peptide residues to either side of P2, P5, and P8 can provide side-chain interactions with DR1 pockets. These pockets, as noted previously in the DR1–HA structure (11), provide subsites for amino acids and determine the peptide-binding motif at positions P1, P4, P6, and P9 (black C-β atoms in Fig. 3). The placement of MHC pockets and distribution of asparagine residues both appear poised to induce the observed ppII peptide conformation.

Conclusions. The electron density observed for a mixture of self-peptides bound to HLA-DR1 is of high quality and has been interpreted as a 13-amino acid peptide. Although self-peptides bound to HLA-DR1 vary greatly in length, the electron density suggests a common conformation for a central core of 13 amino acids, with longer peptides accommodated by extension out of the peptide-binding site. The complexity of the peptide mixture contributing to the observed electron density (Fig. 1) remains unknown. Although there are potentially hundreds of different peptides associated with DR1 derived from LG-2 cells, peptides from the HLA-A2 molecule and the invariant chain occur repeatedly in a range of lengths (from 14 to 24), with each peptide core sequence corresponding to an estimated 13% of the isolated peptide mass (3). However, the electron density shown in Fig. 1 does not simply fit the sequences of either of these two peptides. In addition, recent studies indicate that SEB may selectively bind to a subset of peptide complexes (29) and crystal contacts near the peptide-binding site may also reduce the complexity of the peptide pool in the crystal. The heterogeneity of the observed

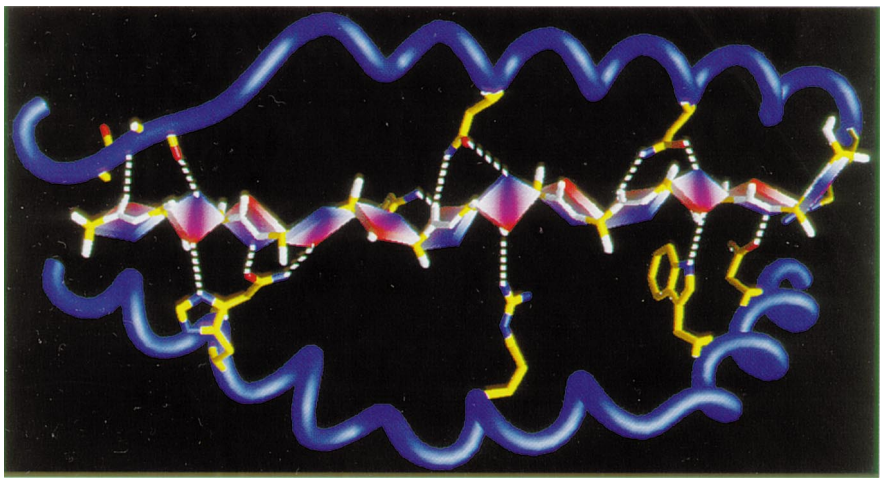

FIG. 5. Hydrogen bonds formed between MHC residues and the peptide main chain. The peptide planes are shown as parallelograms, colored blue near the nitrogen and red near the oxygen of each peptide bond. Superimposed on this are the peptide main-chain atoms in white, except the peptide C-α positions, which are yellow. MHC residues that interact with the peptide are shown, with dotted lines representing hydrogen bonds. Fig. 3 was composed with GRASP (28).

electron density at positions P-1, P8, and the C terminus is consistent with either a mixture of peptides or a mixture of side-chain conformations. In either case, the high quality of the remaining electron density in the peptide-binding site is due to the constraints of the peptide–DR1 interaction. The similarity of the endogenous peptide conformation to the DR1–HA (11) and DR3–CLIP (15) peptide structures further suggests that MHC class II molecules may generally constrain bound peptides to the conformation observed here.

The mechanism by which MHC class II molecules form tightly bound complexes with peptides of diverse sequence is likely to have two components (10, 11). One component would be the MHC pocket interactions with specific side chains of peptides (21–23). Most of the MHC pockets are able to accommodate a number of different side chains, reducing the restrictions placed on the binding of a combinatorial set of peptide sequences. A second component to peptide binding involves conserved MHC residue interactions with the peptide main chain, providing a set of interactions that are independent of the peptide sequence and MHC polymorphism. These interactions may underlie the conserved functional aspects of MHC peptide binding, such as the observed slow dissociation rates of bound peptides. In support of this idea, a minimal 13-mer polyalanine peptide with tyrosine at position P1 (pointing down in Figs. 1, 3, and 5) and lysine at position P5 (pointing out of the binding site in Figs. 1, 3, and 5) can form slowly dissociating complexes with DR1 (23).

A regular distribution of peptide ϕ/ψ angles is observed for the DR1–HA (11), the DR3–CLIP, and the endogenous peptide structures, suggesting that there is a common (and generalizable) conformational constraint placed on the peptide by DR molecules. One potential source of this conformational constraint is the DR interaction with the peptide backbone atoms (Fig. 5). In the HLA-DR peptide-binding site, bidentate hydrogen bonds from three asparagines to the main chain of the peptide are formed and found distributed regularly throughout the peptide-binding site. These asparagine side-chain interactions with a peptide main chain may restrict ϕ/ψ angles even more than β sheet formation, for example, because the cis interaction of the amide side chain should have a more restricted hydrogen-bonding geometry as compared with the ϕ/ψ flexibility of two adjacent peptide segments (Fig. 5). The interaction of other conserved residues forming hydrogen bonds with the peptide main chain, along with the relative placement of MHC pockets, may serve to constrain many peptides to a regular ppII-like conformation.

We thank members of our laboratory, the Cornell High Energy Synchrotron Staff, and the Pittsburgh Supercomputer Center for help in carrying out this work. T.S.J. was supported by the Cancer Research Institute, J.H.B. by the Howard Hughes Medical Institute (HHMI), J.C.G. by the Juvenile Diabetes Foundation International, L.J.S. by a Damon Runyon–Walter Winchell Cancer Fellowship and HHMI, R.G.U. by the Irvington Institute, and J.L.S. by the National Institutes of Health. D.C.W. is an investigator with the HHMI.

1. Germain, R. M. & Margulies, D. H. (1993) *Annu. Rev. Immunol.* **11,** 403–450.
2. Rudensky, A., Preston-Hurlburt, P., Hong, S. C., Barlow, A. & Janeway, C., Jr. (1991) *Nature (London)* **353,** 622–627.
3. Chicz, R. M., Urban, R. G., Laue, W. S., Gorga, J. C., Stern, L. J., Vignali, D. A. A. & Strominger, J. L. (1992) *Nature (London)* **358,** 764–768.
4. Van Bleek, G. M. & Nathenson, S. G. (1990) *Nature (London)* **348,** 213–216.
5. Falk, K., Rotzschke, O., Stevanovic, S., Jung, G. & Rammensee, H. G. (1991) *Nature (London)* **351,** 290–296.
6. Hunt, D. F., Henderson, R. A., Shabanowitz, J., Sakaguchi, K., Michel, H., Sevilir, N., Cox, A. L., Appella, E. & Engelhard, V. H. (1992) *Science* **255,** 1261–1263.
7. Stern, L. J. & Wiley, D. C. (1994) *Structure* **2,** 245–251.
8. Madden, D. R., Gorga, J. C., Strominger, J. L. & Wiley, D. C. (1991) *Nature (London)* **353,** 321–325.
9. Madden, D. R., Garboczi, D. N. & Wiley, D. C. (1993) *Cell* **75,** 693–708.
10. Brown, J. H., Jardetzky, T. S., Gorga, J. C., Stern, L. J., Urban, R. G., Strominger, J. L. & Wiley, D. C. (1993) *Nature (London)* **364,** 33–39.
11. Stern, L. J., Brown, J. H., Jardetzky, T. S., Gorga, J. C., Urban, R. G., Strominger, J. L. & Wiley, D. C. (1994) *Nature (London)* **368,** 215–221.
12. Bouvier, M. & Wiley, D. C. (1994) *Science* **265,** 398–402.
13. Madden, D. R., Gorga, J. C., Strominger, J. L. & Wiley, D. C. (1992) *Cell* **70,** 1035–1048.
14. Guo, H. C., Jardetzky, T. S., Garrett, T. P. J., Lane, W. S., Strominger, J. L. & Wiley, D. C. (1992) *Nature (London)* **360,** 364–366.
15. Ghosh, P., Amaya, E., Mellins, E. & Wiley, D. C. (1995) *Nature (London)* **378,** 457–462.
16. Jardetzky, T. S., Brown, J. H., Gorga, J. C., Stern, L. J., Urban, R. G., Chi, Y.-I., Stauffacher, C., Strominger, J. L. & Wiley, D. C. (1994) *Nature (London)* **368,** 711–718.
17. Brünger, A. T. (1993) XPLOR *Manual* (Yale Univ. Press, New Haven, CT), Version 3.0.
18. Hoffmann, M. L., Jablonski, L. M., Crum, K. K., Hackett, S. O., Chi, Y.-I., Stauffacher, C. V., Stevens, D. L. & Bohach, G. A. (1994) *Infect. Immun.* **62,** 3396–3407.
19. Navaza, J. (1994) *Acta Crystallogr.* **A50,** 157–163.
20. Hammer, J., Takacs, B. & Sinigaglia, F. (1992) *J. Exp. Med.* **176,** 1007–1013.
21. Hammer, J., Valsasnini, P., Tolba, K., Bolin, D., Higelin, J., Takacs, B. & Sinigaglia, F. (1993) *Cell* **74,** 197–203.
22. Sette, A., Sidney, J., Oseroff, C., del Guercio, M. F., Southwood, S., Arrhenius, T., Powell, M. F., Colon, S. M., Gaeta, F. C. A. & Grey, H. M. (1993) *J. Immunol.* **151,** 3163–3170.
23. Jardetzky, T. S., Gorga, J. C., Busch, R., Rothbard, J., Strominger, J. L. & Wiley, D. C. (1990) *EMBO J.* **9,** 1797–1803.
24. Feng, S., Chen, J. K., Yu, H., Simon, J. A. & Schreiber, S. L. (1994) *Science* **266,** 1241–1247.
25. Kraulis, P. J. (1991) *J. Appl. Crystallogr.* **24,** 945–949.
26. Adzhubei, A. A. & Sternberg, M. J. E. (1993) *J. Mol. Biol.* **229,** 472–493.
27. Le Questel, J. Y., Morris, D. G., Maccallum, P. H., Poet, R. & Milner-White, E. J. (1993) *J. Mol. Biol.* **231,** 888–896.
28. Honig, B. & Nicholls, A. (1995) *Science* **268,** 1144–1149.
29. Thibodeau, J., Cloutier, I., Labreque, N., Mourad, W., Jardetzky, T. & Sékaly, R.-P. (1994) *Science* **266,** 1874–1878.